The Role of Continental Heterogeneity on the Evolution of Continental Margin Topography at Subduction Zones

Antoniette Greta Grima (antoniettegreta.grima@glasgow.ac.uk) and Thorsten W. Becker (twb@ig.utexas.edu)

Highlights

The Role of Continental Heterogeneity on the Evolution of Continental Margin Topography at Subduction Zones

Antoniette Greta Grima, Thorsten W. Becker

- We use free-surface subduction models to investigate the influence of heterogeneity across the continental overriding plate.
- Continental structure modulates overriding plate topography, continental extension, trench retreat, and slab morphology.
- Variations in the type of continental heterogeneity can explain variations in the width, extent of extension, and asymmetry of back-arc basins.

The Role of Continental Heterogeneity on the Evolution of Continental Margin Topography at Subduction Zones

Antoniette Greta Grima[a], Thorsten W. Becker[b,c,d]

[a] *School of Geographical and Earth Sciences, University of Glasgow, School of Geographical and Earth Sciences, University of Glasgow, Molema Building, Lilybank Gardens,, Glasgow, G128QQ, United Kingdom*

[b] *Institute for Geophysics, Jackson School of Geosciences, The University of Texas at Austin, J.J. Pickle Research Campus, Bldg. 196 10100 Burnet Road, Austin, TX 78758-4445, Texas, USA*

[c] *Department of Earth and Planetary Sciences, Jackson School of Geosciences, The University of Texas at Austin, 2275 Speedway Stop C9000, Austin, Austin, TX 78712-1722, Texas, USA*

[d] *The Oden Institute for Computational Engineering & Sciences, The University of Texas at Austin, 201 E 24th Street, Austin, Austin, TX 78712-1229, Texas, USA*

Abstract

The nature of the overriding plate plays a major role in shaping subduction zone processes. In particular, the highly heterogeneous continental lithosphere modulates intra-plate tectonics and the surface evolution of our planet. However, the role of continental heterogeneity is relatively under-explored for the dynamics of subduction models. We investigate the influence of rheological and density variations across the overriding plate on the evolution of continental lithosphere and slab dynamics in the upper mantle. We focus on the effects of variations in continental margin and keel properties on deformation, topographic signals, and basin formation. Our results show that the thickness, extent, and strength of the continental margin and subcontinental keel play a crucial role for the morphology and topography of the

overriding plate, as well as the retreat of the subducting slab. We show that this lateral heterogeneity can directly influence the coupling between the subducting and overriding plate and determine the partitioning of plate velocities across the overriding plate. These findings suggest that back-arc extension and subsidence are not solely controlled by slab dynamics but are also influenced by continental margin and keel properties. Large extended back-arc regions, such as the Pannonian and Aegean basins, may result from fast slab rollback combined with a weak continental margin and a strong and extended continental keel. Narrow margins, like the Okinawa Trough in NE Japan, may indicate a comparatively stronger continental margin and weaker or smaller continental keel. Additionally, continental keel properties may affect the overall topography of the continental lithosphere, leading to uplift of the deformation front and the formation of intermontane basins.
Keywords: Continental margin topography, continental heterogeneity, back-arc extension, subduction zone evolution

1. Introduction

The presence of thick, buoyant continental lithosphere at subduction zones is a key feature of modern-day plate tectonics and exerts a first-order control on the subduction zone evolution, the trench rollback behaviour, the slab dip angle at trench, and the slab deflection at the top of the lower mantle (Capitanio et al., 2010; Butterworth et al., 2012; Sharples et al., 2014; Holt et al., 2015a,b; Crameri and Lithgow-Bertelloni, 2018). The continental lithosphere consists of thick, buoyant crust resisting recycling and is often underlain by strong, depleted mantle lithosphere and confined by weak, deformable margins (Jordan, 1981; Lenardic et al., 2000). Results from geopotential, seismic, tomographic, geochemical and rock physics studies show great variability across the continental lithosphere from its margin to its interior domains (e.g. Jordan, 1981; Ghosh et al., 2010; Audet and Bürgmann, 2011; Pearson et al., 2021).

Continental margins are regions of high strain rates, accommodating within their deformation most of the relative plate motions (e.g. Gordon, 2000; Zhong, 2001; Becker, 2006; Ghosh et al., 2013). At subduction zones the margin records the history of subduction and deformation (Uyeda, 1982). Based on estimates of upper plate strain derived from the type of earthquake focal mechanisms, Heuret and Lallemand (2005) and Lallemand and Heuret (2017) broadly classified the deformation of the overriding plate margin into either back-arc extension or compression. Previous work suggests that this dichotomy of back-arc behaviour may be governed by a variety of subduction parameters, such as the convergence velocity, trench rollback, the direction of motion of the overriding plate, the degree of plate coupling at the trench (determined by the strength of the subduction interface), the subducting plate age and the angle of subduction at the trench (Sleep and Toksöz, 1971; Chase, 1978; Molnar and Atwater, 1978; Heuret et al., 2007; Sdrolias and Müller, 2006; Sternai et al., 2014; Sharples et al., 2014).

Continental cratons or continental “roots”, make up a major component of the continental lithosphere and these are understood to be old, thick, cold, and chemically distinct due to their fractionation (Jordan, 1981; Lee et al., 2005). For a planet with active plate tectonics, continental cratons are intriguing in that they have resisted subduction through many Wilson Cycles. This implies that they have to be not only neutral or positively buoyant, but also relatively high viscosity to resist recycling (Lenardic et al., 2000, 2003; Rolf and Tackley, 2011; Yoshida, 2012). Deeply penetrating roots underneath cratonic shields can increase the coupling between the lithosphere and the mantle and modify surface deformation style (Zhong, 2001; Conrad and Lithgow-Bertelloni, 2006; Becker, 2006; O'Driscoll et al., 2009; Paul et al., 2023).

Significant numerical and analogue modelling efforts have sought to understand the role of the continental lithosphere at subduction zones with dynamic subduction models (e.g. Capitanio et al., 2010; Butterworth et al., 2012; Sharples et al., 2014; Holt et al., 2015a,b; Crameri and Lithgow-Bertelloni, 2018; Wolf and Huismans, 2019). However, in most of these studies, the authors consider the overriding plate as homogeneous lithosphere, ignoring the dichotomy between margin and keel. Yet, work by Naliboff et al. (2009), Ghosh et al. (2013), and Paul et al. (2023), for example, suggests that regional variations in lithospheric strength may play an important role in determining the regional stress patterns which has implications for the surface deformation and plate driving forces.

In this work we seek to expand on previous efforts to understand the role of continental strength heterogeneities by exploring the effects of variations in continental margin and keel properties on the evolution of deformation, topographic signal, and basin formation in a 2-D numerical model of subduction with and without a free surface boundary condition. Expanding on the back-arc deformation studies for a homogeneous overriding plate by Balázs et al. (2017), Wolf and Huismans (2019), Dasgupta et al. (2021), and Erdős et al. (2022) we show that continental deformation and back-arc extension can occur in both wide and narrow continental back-arcs, and is controlled to a large extent by the thickness, extent, and strength of the continental margin and the continental keel. The nature of this heterogeneity influences the extent, depth, and asymmetry of deformation and subsidence within the continental back-arc region, and the amount of trench retreat observed on the subducting plate.

2. Methods

2.1. Modelling approach

Building on earlier studies, we model freely evolving subduction and interactions with an overriding plate within the approximation of a thermo-mechanical, 2-D convective system (Holt et al., 2015a; Holt and Condit, 2021). For this, we use the finite element code ASPECT (version 2.3.0) (Kronbichler et al., 2012; Heister et al., 2017; Bangerth et al., 2021) to solve the equations for the conservation of mass (eq. 1), momentum (eq. 2) and energy (eq. 3) to model flow of an incompressible, laminar fluid under the

Boussinesq approximation and no internal heating:

$$\nabla \cdot \mathbf{v} = 0 \tag{1}$$

$$-\nabla \cdot (2\eta\dot{\epsilon}) + \nabla p = \rho\mathbf{g} \tag{2}$$

$$\left(\frac{\partial T}{\partial t} + \mathbf{v} \cdot \nabla T\right) - \kappa \nabla^2 T = 0 \tag{3}$$

Here, $\mathbf{v}$ is the velocity, $\dot{\epsilon}$ is the strain-rate tensor, η viscosity, p pressure, $\mathbf{g}$ gravitational acceleration, T temperature, and κ thermal diffusivity. Our basic setup builds on Holt and Condit (2021), and Table 1 provides more details on the model parameters used in this study.

2.1.1. Numerical parameters and boundary conditions

Our subduction models evolve dynamically self-consistently in that there are no external forces or velocities applied to the system. Our model domain extends to 11,600 km in the x-direction and 2,900 km in the y-direction (Fig. 1). Our side boundaries are free slip and our top boundary is a free surface which allows for self-consistent mesh deformation and topographic build-up with model evolution. We also include model suites with a mechanical free slip top boundary condition to compare the role of the free surface in the evolution of overriding plate topography and slab dynamics (Table A.2 and Figs. A.10-A.13). For our free surface models, we choose to advect the

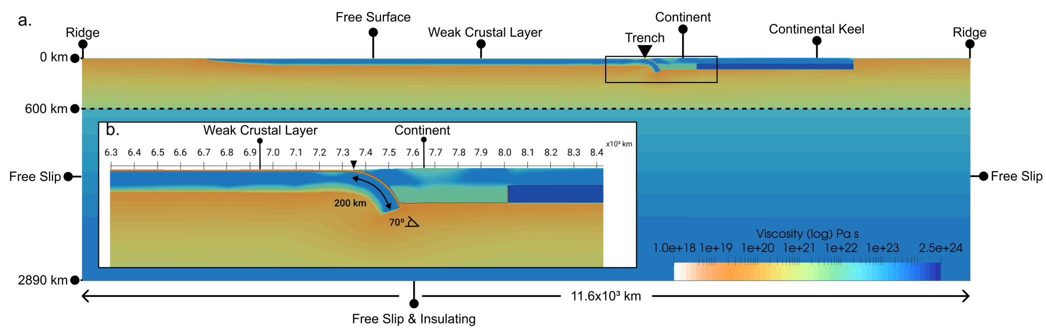

Figure 1: a) Model set-up including a free surface top boundary condition and a continental keel with inset, b), showing a zoomed-in view of the subducting and overriding plates, the weak crustal layer, and the initial condition of our model at the start of our models for reference-keel case 4.

free surface in the direction of the surface normal (instead of that of the local vertical) to avoid mesh distortions and better mass conservation preservation of the domain. We also apply a diffusion process in order to counteract the strong mesh deformation, in an approach similar to that adopted by Sandiford et al. (2021). We also limit our initial maximum time step (to 200 years), the relative increase in time step (to 20), and the overall maximum time step allowed in the model (to 2,000) to encourage initial isostatic convergence to equilibrium.

We use ASPECT's adaptive mesh refinement (AMR) to increase the resolution of our models around areas of interest, namely around the subducting slab, at the top of the model domain, within the overriding continental lithosphere and around and within a 7.5 km thick weak crust which acts as an interface between the subducting and overriding plates. We do this by setting AMR to occur for finite elements with large gradients in viscosity, temperature, and composition. This allows us to obtain a resolution of 500 m to

1 km within the regions of interest while also modelling flow at the scale of the whole mantle. For models with a free surface top boundary condition, AMR is initiated after the first 0.5 Myr of model evolution. This is to avoid recurring refinement during the free surface oscillations prior to its isostatic stabilisation.

2.1.2. Initial conditions

The initial set-up for our reference case model (keel-free case 1, Table A.2) includes a 6,000 km long, 80 Ma old oceanic lithosphere subducting at an initial subduction angle of 70°, with an initial slab length of 200 km, under a 2500 km long, 150 km thick, 120 Ma, buoyant continental lithosphere (Table 1). Both the oceanic and continental plates are bounded by ridge segments on either side of the model domain and are separated by a 7.5 km thick weak crustal layer (Fig. 1). This crustal layer has viscosity of 10^{20} Pa s and acts to decouple the two plates where the properties of the crustal layer were discussed by Behr et al. (2022).

To test the role of continental heterogeneity on the evolution of subduction and topography, we compare our keel-free case 1 model with our reference-keel case 2 where we implement a 75 km thick, 200 km long keel at the bottom of the continental lithosphere (Fig. 1). The continental keel starts at 200 km away from the edge of the continental lithosphere at the trench and extends all the way under the remaining extent of the overriding plate. In our models, the keel strength is represented by a viscosity increase from 10^{23} Pa s (which is the standard viscosity of the continental lithosphere in our models) to 10^{24} Pa s. The weak crustal layer, the continental overriding plate, and the continental keel are implemented and advected as separate compositional fields, which are discussed next.

2.1.3. Temperature and density structure

The lithospheric plates in our models are defined using the half-space cooling law for lithosphere of 80 Ma and 120 Ma respectively, we use a thermal diffusivity of 10^{-6} m^2s^{-1} and a mantle potential temperature of 1573 K. The density in our models is temperature dependent and we include different reference densities for the background mantle and oceanic lithosphere, the overriding continental plate and continental keel, and the oceanic crust (Table 1). In the reference-keel cases (cases 2 and 4), the continental plate and continental keel have the same density but this is modified for some specific test cases (Table A.2). The crust and the overriding plate material have lower densities compared to the oceanic lithosphere and mantle which is to ensure a positively buoyant continental plate and to approximate the lower density of the basaltic crust similar to the approach adopted by Behr et al. (2022).

Parameter	Symbol	Units	Value
Thermal expansion coefficient	α	K^{-1}	$3 \cdot 10^{-5}$
Thermal diffusivity	κ	m^2s^{-1}	10^{-6}
Surface temperature	T_s	K	273
Mantle potential temperature	T_m	K	1573
Adiabatic temperature gradient	d_zT	K km^{-1}	0.3
Slab and mantle density	ρ_0	kg m^{-3}	3300
Weak Crust density	ρ_{crust}	kg m^{-3}	3175
Continental and keel density	ρ_{op}	kg m^{-3}	3150
Gravitational acceleration	g	m s^{-2}	9.8
Subducting plate age	t_{sp}	Myr	80
Subducting plate viscosity	η_{sp}	Pa s	$2.5 \cdot 10^{22-23}$
Weak Crust viscosity	η_{crust}	Pa s	$2.5 \cdot 10^{20}$
Weak Crust thickness	h_{crust}	km	7.5
Overriding plate age	t_{op}	Myr	120
Overriding plate viscosity	η_{sp}	Pa s	$2.5 \cdot 10^{22-23}$
Overriding plate thickness	h_{op}	km	150
Reference keel viscosity	η_{keel}	Pa s	$2.5 \cdot 10^{24}$
Reference keel thickness	h_{op}	km	75
Maximum viscosity	η_{max}	Pa s	$2.5 \cdot 10^{24}$
Minimum viscosity	η_{min}	Pa s	$2.5 \cdot 10^{18}$
Dislocation creep (UM)			
Activation energy	E	$kJmol^{-1}$	540
Activation volume	V	cm^3mol^{-1}	12
Pre-factor	A	$Pa^{-1}s^{-1}$	$8.5 \cdot 10^{-15}$ (LM)
Exponent	n	-	3.5
Diffusion creep (UM,LM)			
Activation energy	E	$kJmol^{-1}$	300 (UM,LM)
Activation volume	V	$cm^3mol{-}1$	4 (UM), 2.5 (LM)
Pre-factor	A	$Pa^{-1}s^{-1}$	10^{-10} (UM), $5.78 \cdot 10^{-13}$ (LM)
Exponent	n	-	1
Plastic yielding			
Friction coefficient	a	-	0.6
Cohesion	b	MPa	60
Pore fluid factor	λ	-	0.15
Maximum yield stress	τ_{max}	MPa	600

Table 1: Model parameters

2.2. Rheology

The rheology of the mantle in our models is determined by a composite creep law which combines diffusion creep, dislocation creep, and plastic yielding (Billen and Hirth, 2005; Becker, 2006; Garel et al., 2014). For the upper mantle, we use the following creep laws:

$$\eta_{diff/disl} = A^{\frac{1}{n}} \dot{\epsilon}_{II}^{\frac{1-n}{n}} \exp \frac{E + PV}{nRT}, \tag{4}$$

Where η is the composite viscosity, A a pre-factor, $\dot{\epsilon}_{II}$ the second invariant of the strain rate tensor, n the stress exponent, R the gas constant, P the lithostatic pressure, and T temperature. Our choices of parameters (Table 1) are consistent with experimental values for olivine (e.g. Hirth and Kohlstedt, 2004). We include a 0.3°C km^{-1} adiabatic temperature gradient for T in eq. (4), and set the diffusion and dislocation creep pre-factors to give η_{diff} $= \eta_{disl} = 5 \cdot 10^{20}$ Pa s at a transition strain rate of $5 \cdot 10^{-15}$ s^{-1} and depth of 330 km (*cf.* Billen and Hirth, 2005; Becker, 2006). We increase the viscosity of the lower mantle by a factor of 20 as motivated by geoid constraints (e.g. Hager, 1984; King and Masters, 1992) and limit deformation in the lower mantle to occur only through diffusion creep.

We include quasi-plastic behavior by approximating brittle yielding at lithospheric depths, defined as

$$\eta_{yield} = \frac{\min(\tau_{yield}, 0.5\text{GPa})}{2\dot{\epsilon}_{II}}, \tag{5}$$

where τ_{yield} is approximated by a Coulomb friction criterion

$$\tau_{yield} = (a\sigma_n + b)\lambda. \tag{6}$$

Here, a is the friction coefficient (0.6), b is the cohesion (60 MPa), λ is the pore fluid factor also known as the yielding pre-factor and is defined as (e.g. Enns et al., 2005)

$$\lambda = 1 - \frac{P_{fluid}}{P_{rock}} \tag{7}$$

For our reference model λ has a value of 0.15 but we increase this value to 0.3 and decrease it to 0.07 for our reduced and increased plastic yielding cases respectively (Table A.2). Similar to previous work we assume that σ_n is equal to the lithostatic pressure P.

The effective viscosity is then calculated as

$$\eta_{eff} = \left(\frac{1}{\eta_{diff}} + \frac{1}{\eta_{disl}} + \frac{1}{n_{yield}} \right)^{-1} \tag{8}$$

and is additionally bounded between an upper limit of $2.5 \cdot 10^{24}$ and a lower limit of $2.5 \cdot 10^{18}$ Pa s to encourage model convergence.

2.3. Model parameters and variations

We compare our keel-free case 1 and our reference-keel case 2 (sec. 2.1.2) against variations in continental lithosphere strength. We first include a 75 km weak layer at the bottom of the continental lithosphere (keel-free case 3) to approximate a rheologically weaker lower continental crust. Next, for keel case 4 we combine this weaker lower continental lithosphere with a strong continental keel. This set-up describes a continental margin with a weak lower continental crust and a continental interior underlain by stronger continental lithosphere. For cases 1-4 we test each set-up using a free surface and a free slip top boundary condition (Table A.2).

To explore the effect of the continental keel properties on the evolution of topography and slab morphology we then vary the properties of the continental keel by changing its thickness (cases 5 and 6), extent (keel-case 7), density (keel-case 8), and viscosity (keel-cases 9 and 10; Table A.2). We also vary the continental margin properties by decreasing the keel-free margin extent (margin-case 11), varying its thickness (margin-case 12), and changing the amount of yielding allowed (margin-cases 13 and 14; Table A.2).

2.4. Model analysis

For each model we track; i), the average overriding and subducting plate velocities (measured within the plate core and averaged over the length and depth of the plate), ii), the convergence velocity, iii), the velocity of the sinking slab and the induced return flow in the upper mantle, iv), the viscosity, stress, strain rate, and temperature evolution, and, v), the topographic evolution.

We also measure the slab dip angle θ at 175 km depth

$$\theta = \tan^{-1} \frac{\delta y}{\delta x}, \tag{9}$$

where δy is the depth measured between 175 km at the surface and the slab tip if this is above 400 km depth or at 400 km depth if the slab tip has sunk into the mantle transition zone. δx describes the horizontal distance between the top of the slab at 175 km depth and the slab tip.

The velocity V_{tr} of the subducting plate at the trench is defined here as the deepest point on the subducting plate located away from the ridge and is described by

$$V_{tr} = \frac{V_{stokes}}{\tan\theta}, \tag{10}$$

where V_{stokes} is the vertical velocity of the slab measured directly from the model output and θ is the slab dip angle at 175 km depth (eq. 9).

We also define a deformation extent within the overriding plate. This region describes the keel-free margin of the continental lithosphere. For this region, we track the change in thickness, horizontal extent, strain rates, and viscosity from the model output. Our convergence rate is calculated based on the velocity of the subducting lithosphere, the trench, the deformation region, and the velocity of the continental craton (defined as that part of the continental lithosphere overlying by the continental keel). We also track the amount of trench rollback for every 0.5 Myr of model time. Lastly, we qualitatively examine the slab morphology within the upper mantle and at 660 km depth.

3. Results

3.1. Surface boundary conditions, topography, and dynamics

Since we seek to evaluate topography predictions, we test a range of model set-ups (Table A.2) with both a free surface and a free slip top boundary to compare the influence of the boundary condition on the slab morphology, the strain rates and the topography generated on the overriding plate (Fig. 2). For all cases, there is little variation in the slab morphology in the upper and lower mantle across the free surface and free slip implementations, as expected (Kaus et al., 2008).

Strain rates and surface topography are also comparable save for minor, small-scale features (Figs. 2, A.10-A.11) for keel-free case 1 and the keel case 2. However, for keel-free case 3 and keel case 4, when introducing vertical and lateral heterogeneity within the overriding continental plate, the type of surface boundary condition becomes important for surface deformation and topography. For these cases, the free surface implementation exhibits focusing of higher strain rates within the continental lithosphere for the first 30 Myrs of model evolution (cf. Crameri and Lithgow-Bertelloni, 2018) and produces significantly different topographic signals compared to the free slip version of the same set-up (Fig. 2). However, similar to cases 1 and 2, the slab morphology in cases 3 and 4 is unaffected by the nature of the top boundary condition, indicating that the type of boundary condition at the surface of the model does not play a significant role in the evolution of slab morphologies (Figs. 2, A.10-A.13; cf. Kaus et al., 2008). For the rest of

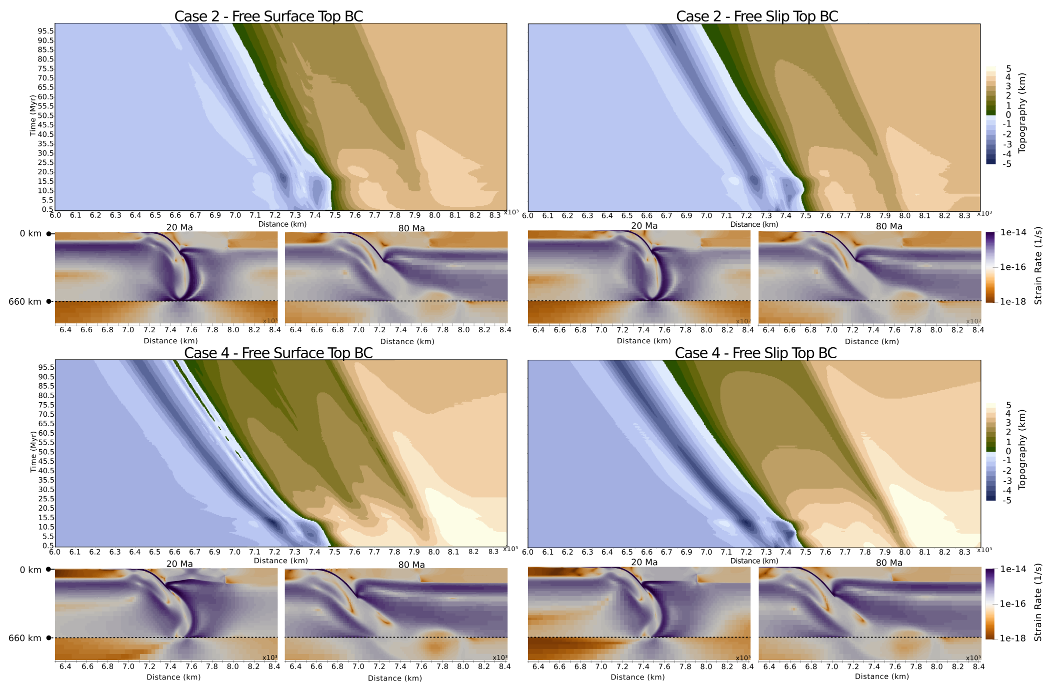

Figure 2: Surface boundary conditions tests. Top six panels show results form reference-keel case 2 with homogeneous continental η and continental keel implementation. Left: Free surface boundary condition. Right: Free slip boundary condition. Top row: Topography as a function of horizontal distance and time; bottom row: strain rates and slab configuration for two timesteps. Bottom six panels show the same fields for keel case 4 with continental η variations and keel implementation.

the paper we will focus on models which include the computationally more challenging, but more realistic free surface top boundary condition.

3.2. Continental keel variations

Comparing keel-free case 3 and keel case 4 (Figs. A.12 vs. A.13) it is clear that the presence of a higher viscosity continental keel underneath the continental interior makes an important contribution to the return flow within the upper mantle, the slab morphology, the location of deformation and the overall evolution of topography on the overriding plate. The keel in case 4 encourages strain rate focusing within the continental margin, resulting in a centralized zone of subsidence bounded by two shoulders of higher topography on either side of the margin, mimicking "horst" and "graben" structures. This topographic signal forms early on in the model evolution and is maintained through the model run. However, does the nature of the lateral heterogeneity introduced by the continental keel matter? To answer this question we first vary the geometry and then the rheology of the continental keel and compare the topographic signal, the strain rates within the continental plate and the slab morphology.

3.2.1. Geometry variations

Increasing the continental keel thickness (keel-case 5, Fig. 3 and Table A.2) does not result in significant differences in model behaviour and topographic signal. However, the subsidence within the central basin of the continental margin for this case, is both narrower and deeper compared to that observed for keel-case 4 (Table A.3). Decreasing the continental keel thickness (keel-case 6) results in a significantly steeper slab in the upper mantle and a reduced trench retreat. Case 6 records overall shallower topographic elevations, increased tilting of the entire overriding plate towards the trench and a distinct lack of the horst and graben morphology which is observed within the continental margin region of the two previous cases (Fig. 3, Table A.3). Maintaining a standard keel thickness and extending its length in keel-case 7 (Fig. 3) encourages slab flattening. Significant subsidence within the continental margin results, and a wide deformation front forms. The margin deformation is characterised by a central zone of extension split into 3 focused zones of subsidence. This zone of extension (Table A.3) is bounded by two areas of higher elevation similar to previous models with the same or higher keel thickness (cases 4 and 5). Extending the continental keel (Fig. 3) also encourages the opening of multiple basins within the continental margin increasing the amount of margin extension and produces an overall deeper trench across the entire model evolution when compared to the previous 3 cases (Table A.3).

3.2.2. Rheology variations

We next maintain the same keel geometry, but change its density in case 8 and viscosity in case 9 (Fig. 4 left and central panels and Table A.2). Introducing a continental keel with a higher density (Table A.2), results in isostatically increased elevations within the deformed continental margin and lower elevations within the continental interior. Despite the inversion of the typical topographic signal between the margin and the continental interior we still observe a focused center of subsidence within the continental margin. At its deepest the central basin of keel-case 8 is considerably narrower compared to previous models but it is similarly bound by two fronts of higher elevation (Fig. 4 and Table A.3).

In keel-case 9 we maintain the reference keel density but increase its

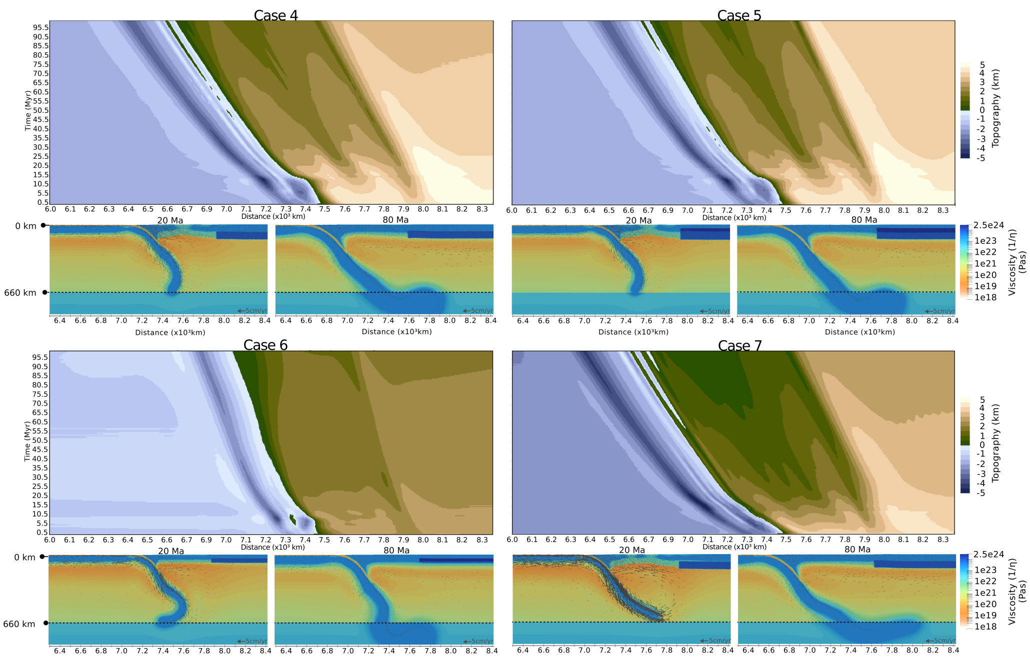

Figure 3: Effect of continental keel geometry: case 4 (top left) with standard continental keel; case 5 (top left) with thick continental keel; case 6 (bottom left) with thin continental keel; case 7 (bottom right) with extended continental keel. Layout and subplots are similar to Fig. 2, but we now show viscosity and flow velocity at different timesteps in the small subpanels.

viscosity by two orders of magnitude (Table A.2). The margin exhibits similar topographic patterns to those observed in cases 4, 5, 7, and 8 with typical horst and graben signatures. Both cases 8 and 9 show similar slab behaviour in the upper and lower mantle which is consistent with that observed for previous cases (Fig. 4).

Lastly, in keel-case 10 we combine the extended keel of case 7 with the higher viscosity keel of case 9. We note very similar behaviour to case 7 with the development of an extensive and wide deformation front along the continental margin. Similar to case 7, keel-case 10 also exhibits multiple basins within a central zone of subsidence along the continental margin. These are the deepest basins recorded across all models. Trench retreat is significant throughout the model evolution and the considerable slab rollback results in slab flattening at 660 km depth. After travelling horizontally at the top of the lower mantle the deflected slab eventually sinks below 660 km depth. This behaviour coincides with the a secondary phase of subsidence within continental margin during the later stages of the model evolution (Fig. 4).

3.3. Continental margin variations

3.3.1. Geometry effects

We next vary the properties of the continental margin. For margin-case 11 (Fig. 5) we decrease the margin extent and maintain the standard keel properties of keel-case 4 (Fig. 3). We observe that the narrower margin is sig-

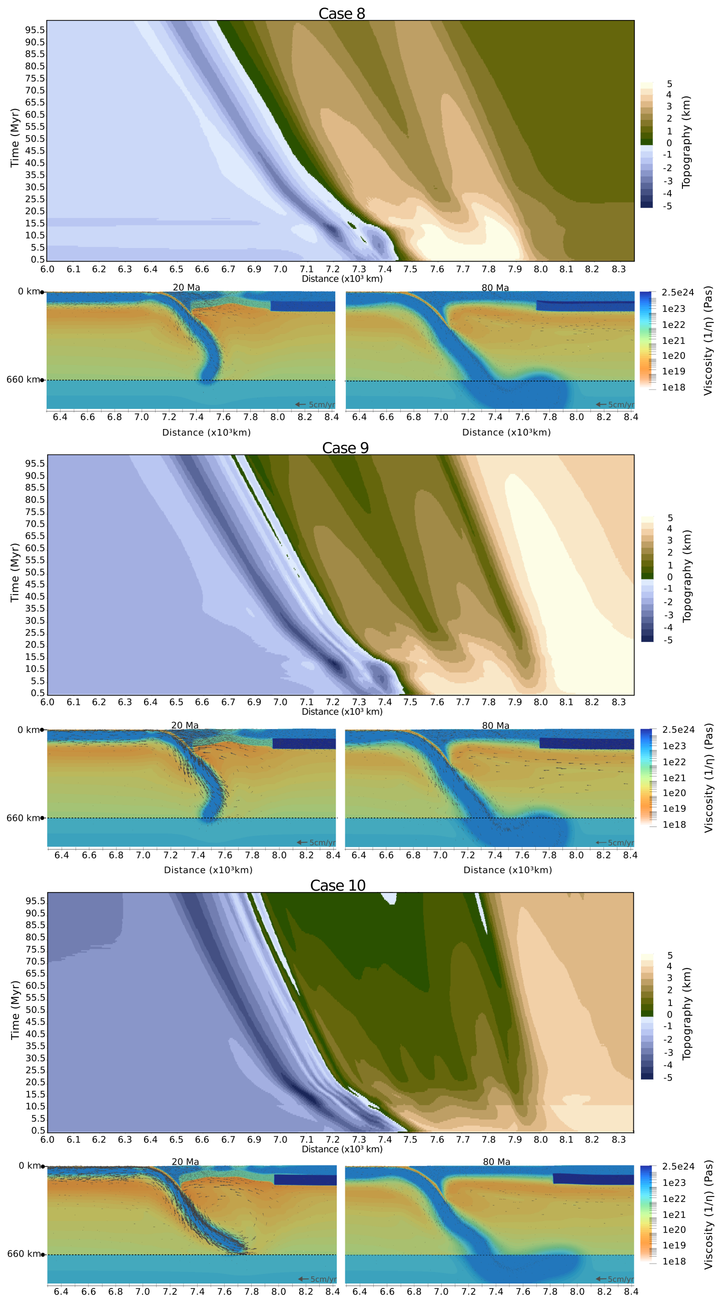

Figure 4: Effect of continental keel rheology: case 8 (left) with a neutrally buoyant continental keel; case 9 (centre) with a higher η of 10^{26} Pa s and case 10 (left) with an extended, 900 km, 10^{26} Pa s η keel. Top row: Topography; bottom row: viscosity and induced viscous flow velocity

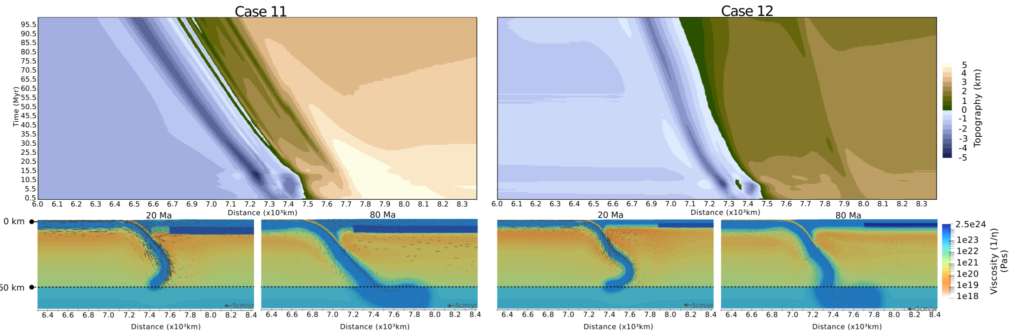

Figure 5: Effect of continental margin geometry: case 11 (left) with a thin margin and standard continental keel; case 12 (right) with thin margin and keel. Top row: Topography; bottom row: viscosity and induced viscous flow velocity

nificantly more deformed than in previous cases, and hosts three narrow and long basins within the central zone of deformation and along the edge margin closest to the keel. The slab morphology is steeper than that observed for previous cases and matches that of keel-case 6. Combining a thin margin and keel (margin-case 12, Fig. 5) results in smooth overriding plate topography without the characteristic regions of uplift and extensive basin nucleation common to the previous cases. This is similar to the topographic signal recorded in keel-case 6 (Fig. 3). Case 12 shows transient, minor subsidence along a narrow ledge between the margin and the continental keel, a steep slab, limited trench rollback (Table A.3) and widespread tilting of the continental overriding plate towards the trench (Fig. 5).

3.3.2. Rheology effects

We next test the effect of rheology (Fig. 6). Models have a standard keel but for margin-case 13 the amount of plastic yielding allowed within the continental lithosphere (excluding the keel) is reduced by changing λ from 0.15 to 0.3 (cf. Enns et al., 2005). In case 13 a central uplift trend within the continental margin complements the uplift of the continental interior for the first 15 Myrs of model evolution (Fig. 6). However, after 20 Ma the topography within the margin decreases. This subsidence trend continues throughout the model's middle stages and develops multiple narrow zones of focused subsidence towards the later model stages. A consistent centre of subsidence also develops within the continental margin at the edge of the keel shoulder (Fig. 4 and Table A.3). Contrary to the subsidence recorded in previous models this is not confined to the centre of the margin but rather to its keel-ward edge (Fig. 5). Despite this variation in topographic signal the slab evolution is similar to that observed for cases 4, 5, 8 and 9 (Fig. 6).

In margin-case 14 (Fig. 6) we increase the amount of plastic yielding allowed within the continental lithosphere (excluding the continental keel) by decreasing λ from 0.15 to 0.07. This allows the continental plate to be more easily deformed. Increased plastic yielding results in an extended continental margin with significant subsidence. Subsidence is focused within two main basins which are bound by three regions of higher elevations. These zones of higher topography bind the margin on either side and a central elevated zone separates the two basins. The slab morphology mimics that of keel-cases 7 and 10 with deflection and flattening above 660 km and eventual descent into the lower mantle during the later model stages (Fig. 6).

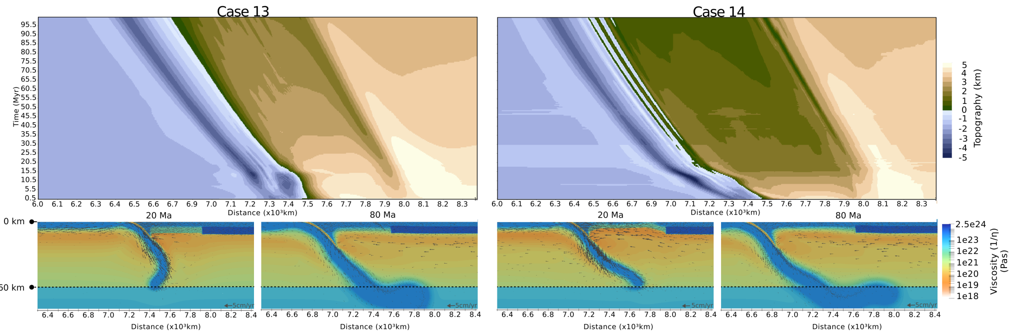

Figure 6: Effect of variations in continental deformation: case 13 (left) with reduced continental plastic yielding and standard continental keel; case 14 (right) increased continental plastic yielding. Top row: Topography; bottom row: viscosity and induced viscous flow velocity

3.4. The influence of continental heterogeneity on trench retreat and the extent of continental margin deformation

The presence of heterogeneity in the continental lithosphere thus influences the morphology and topography of the overriding plate, and the trench retreat of the subducting lithosphere. Keel geometry and rheology can play a role on both the extent and amplitude of the deformation experienced by the continental margin. Fig. 7 shows the amount of trench retreat against the area of deformed and extended continental margin for all keel variations, for the whole model evolution (top), and the upper mantle stages (bottom). There is a linear relationship between the increasing trench retreat and the increase in deformation extent along the continental margin. This is evident in the upper mantle stage of the model evolution (Fig. 7). Comparing model evolution across the entire model run, models whose keel geometry varies tend to slightly favour increases in trench retreat over increases in the extent of deformation (Fig. 7). Models where the keel rheology varies tend to exhibit slightly bigger increases in the margin deformation front compared to the trench retreat.

Fig. 7 shows that the keel influence on the overriding plate can be grouped into three broad categories. Models with limited keel influence (group A) exhibit a restricted deformation extent with a very subdued topographic signal, limited extension, and no basin formation on the overriding plate (e.g., keel case 6 and Fig. 7 inset a). The models in group A also have limited trench retreat, and show a steep slab morphology in the upper mantle. In contrast, group C models show both significant trench retreat and extensive deformation along the continental margin. In group C slabs flatten and travel horizontally at 660 km depth until they avalanche into the lower mantle during the later stages of model evolution. These models exhibit multiple basin nucleation events and deep subsidence within the continental margin. Most models, however, sit between these two end members (Group B). The Group B models combine a modest deformation extent along the continental margin with modest to high trench rollback. These models undergo temporary slab anchoring at 660 km depth without the extensive flattening observed for Group C models. A central basin, flanked by two zones of higher topography, is also distinctive of group B models and is reminiscent of horst and graben structures observed in places like the Basin and Range along the North American margin (Table A.3).

For models with margin properties variations we observe a significant dis-

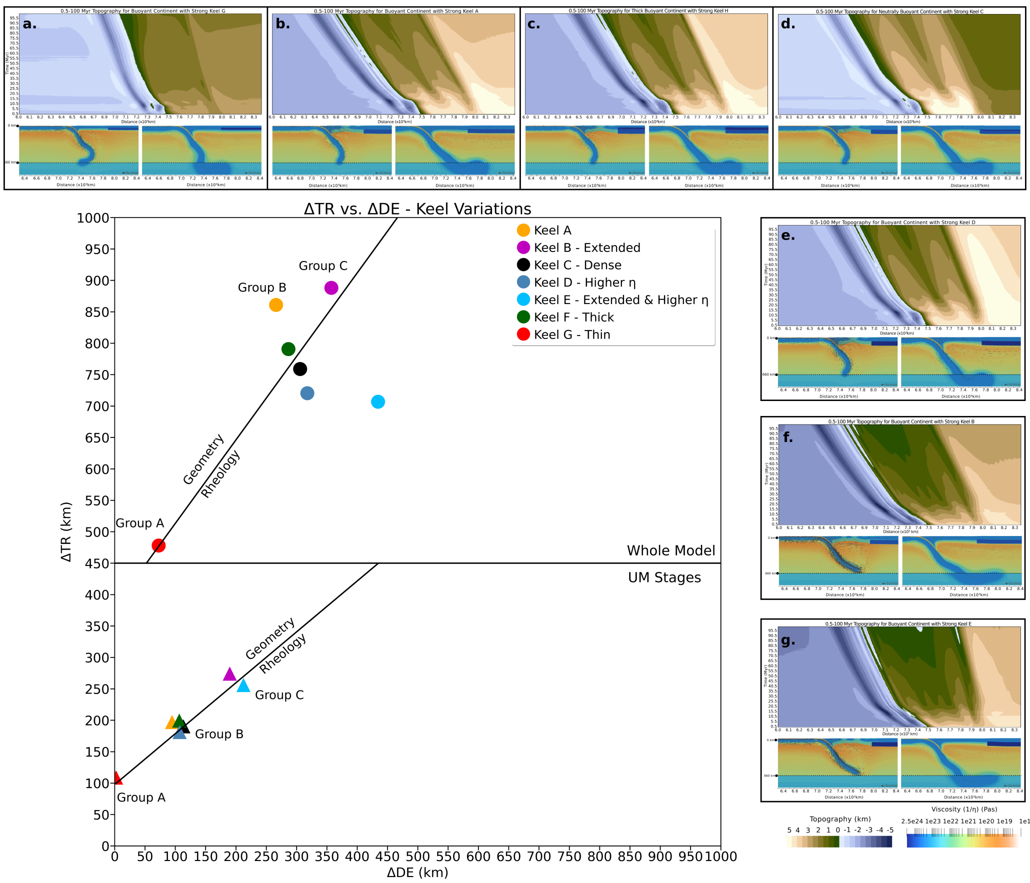

Figure 7: Trench retreat vs. extent of deformation along the continental margin for keel variations for the whole model (top) and upper mantle stages (bottom). Top & right insets: Topography and slab morphology for case 6(a), case 4(b), case 5(c), case 8(d), case 9(e), case 7(f), case 10(g)

tinction between geometry and rheological effects (Fig. 8). Geometry variations result in a spatially limited deformation front and limited to modest trench retreat extents. However, rheological type variations in the continental margin (determined here by the amount of plastic yielding allowed in the model) show a clear trend of increasing trench retreat with a widening of the deformation front on the overriding plate, consistent with the keel variations models discussed above. Models with higher plastic yielding exhibit larger amounts of trench retreat and wider deformation fronts on the overriding plate than those with limited plastic yielding. Higher plastic yielding produces the highest amount of trench retreat and overriding plate margin deformation.

Excluding models with margin geometry variations, where the continental margin deformation is dominated by the spatial limits of the margin itself, the linear relationship exhibited in Figs. 7 and 8 indicates a strong coupling between the subducting plate and the continental margin. This behaviour suggests that the overriding plate margin is being dragged and extended as the slab rolls back and the trench retreats. While it is clear that the subducting slab drives the dynamics of the system, the structure of the overriding plate controls how much of that driving force is partitioned between the slab rollback and the drag of the continent towards the trench. The continental structure also determines where the plate driving forces are partitioned on the overriding plate and spatially limits extent of the subducting plate influence on the overriding plate, discussed next.

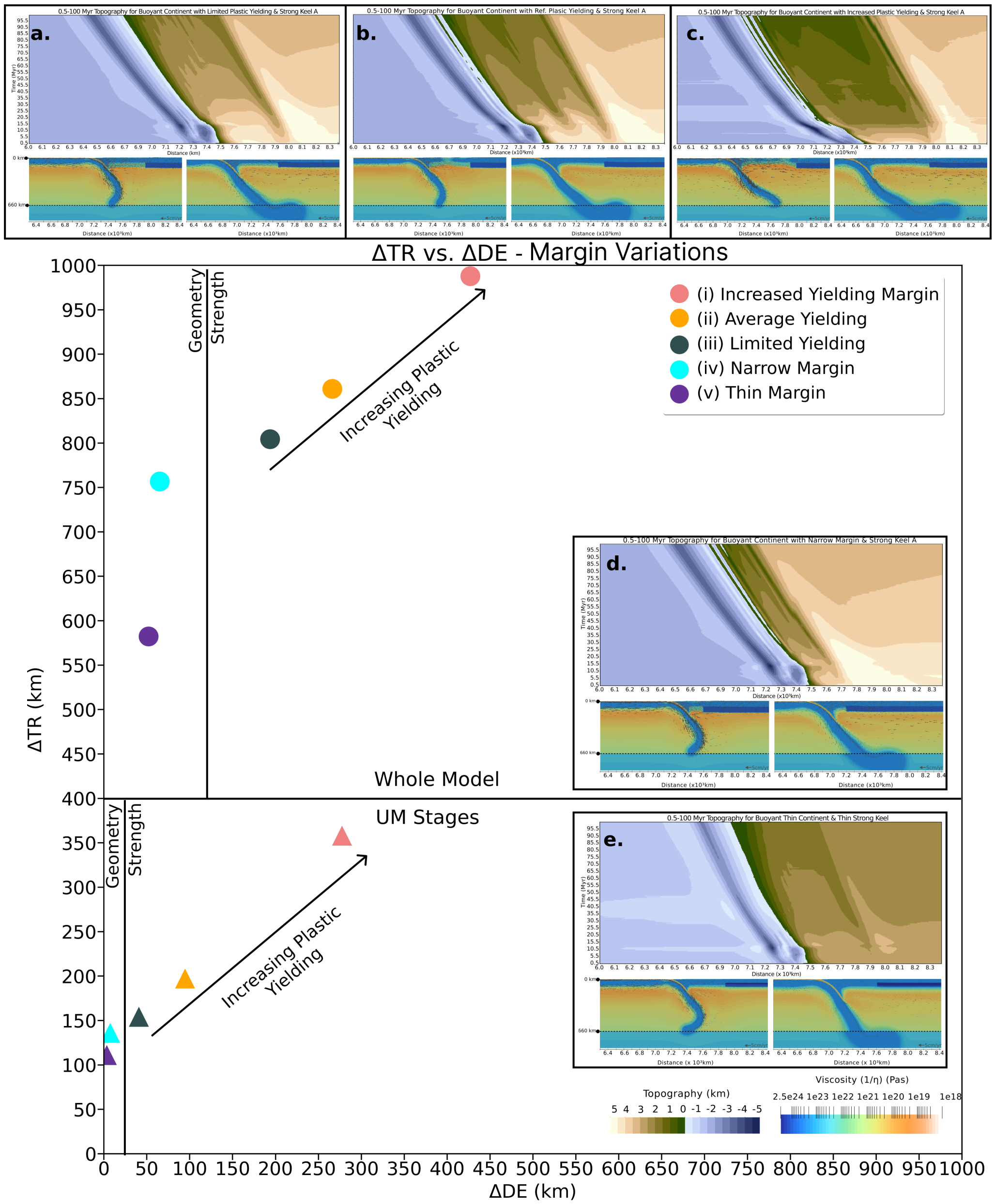

Figure 8: Trench retreat vs. extent of deformation along the continental margin for margin variations for the whole model (top) and upper mantle stages (bottom). Top & right insets: Topography and slab morphology for case 13(a), case 4(b), case 14(c), case 11(d), case 12(e)

3.5. The role of continental heterogeneity and velocity partitioning

For models with a continental keel the subducting slab and continental margin are coupled and their motion is complementary, where both move in the same direction with comparable velocities (Fig. 6). However, the continental interior overlying the continental keel tends to move at considerably slower velocities, if at all (Fig. 9). In these cases there are two competing forces; the drag induced by the slab rollback pulling the weaker margins towards the trench and the stabilising influence of the continental keel which resists it. The end result is strain rate focusing within the continental margin as this is pulled apart by the retreating trench and trench-ward return flow on one side and the stable, slow-moving continental interior on the other side. This is true for all models with a continental keel but this effect is particularly noteworthy in keel-case 7 and margin-case 14 (Fig. 3). In the former, the extended nature of the keel results in an even more stable continental interior and stronger velocity partitioning within the continental margin, while in the latter case, the weaker margin accommodates most of the trench-ward drag of the slab rollback, moving as one with the trench while the continental interior remains mostly unperturbed by the induced slab flow (Fig. A.14).

The way velocity is partitioned within the overriding plate also reflects the slab dynamics in the upper mantle. Extensive trench retreat and wide, extended back-arc basins are associated with slab bending and slab flattening at the top of the lower mantle. This slab behaviour induces stronger return flow within the mantle wedge compared to other slab morphologies (Fig. 9).

The presence of a continental keel forces the induced viscous flow within a narrow zone underlying the continental margin. This exerts an additional drag on the continental margin in the direction of the return flow and towards the trench (cf. O'Driscoll et al., 2009). Fig. 9 shows that when increased yielding within the continental margin (e.g., case 14) is combined with a focused return flow channel, this encourages the formation of four bands of different velocity zones within the continental margin (Fig. 9b, central column and row) with the fastest moving sections of the continental margin found closest to the trench and the slowest moving sections overlap the edge of the stable continental interior. The differential margin velocities overlap with a broad zone of high strain rates bounded by shear bands which delimit the trench-ward and the continental interior sides of the margin (Fig. A.14).

In models with steeper slab morphologies the induced return flow within the mantle wedge is considerably weaker and its extent smaller. However, despite the limited extent and magnitude (when compared to deflected slab cases) the induced viscous flow for these models (e.g., cases 4, 5, 8, and 9) is still channeled by the keel into a narrow higher velocity band underneath the continental margin and thus also contributes to the drag that is pulling the margin towards trench. Fig. 9 a illustrates how the velocity within the continental margin is split, with the faster trench-ward edge of the margin overlying the zone of faster channel return flow within mantle wedge. Fig. 9 also shows that the split in velocities corresponds to a zone of localized strain-rates within the central axis of the margin. This strain focusing allows for the nucleation of subsidence within the margin into a central basin (Fig. A.14).

Models with thin keels and margins do not exhibit this relationship between the trench retreat and the continental margin extent. Fig. 9c shows that there is no velocity differentiation across the thin continental margin or the continental interior. Despite the fast slab sinking velocities exhibited by the slab, the induced return flow is weak and the thin continental keel is ineffective at focusing the induced mantle flow into a narrow high-velocity channel observed in the previous models. This indicates that the presence of a thick continental keel enhances and focuses the induced viscous flow in the mantle wedge into a high-velocity channel directly underlying the continental margin effectively dragging the continental margin towards the trench (cf. O'Driscoll et al., 2009; Paul et al., 2023). For thin continental keels and margins the return flow within the mantle wedge is weaker and spread over a wider area underneath the entire continental overriding plate. In these cases the continental keel is ineffective at channeling the return flow and we see no partitioning of the velocities within the continental margin or between the continental margin and the interior. In such cases, the slab-induced flow is not partitioned across the overriding plate and the continental margin and interior move coherently and at the same velocity. As a result there are no "pull-apart" forces acting on the margin, and therefore no extension and subsidence.

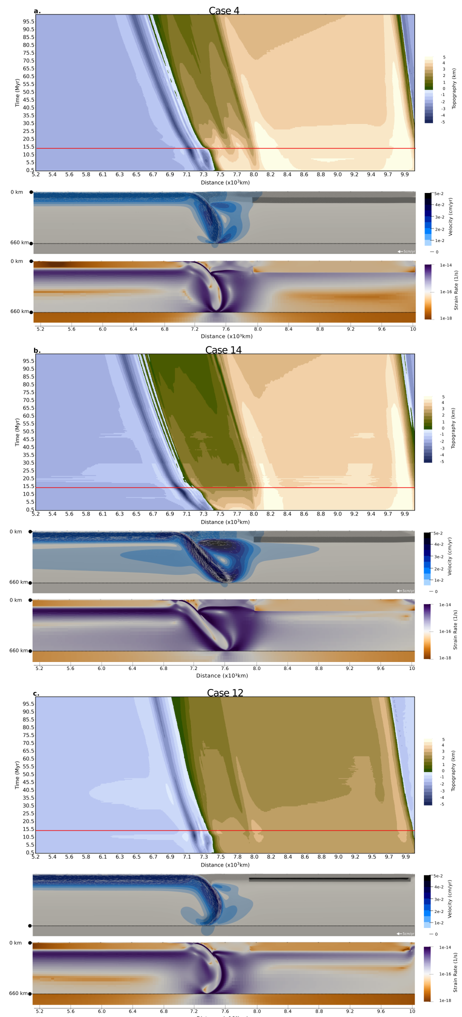

Figure 9: Top row: free surface topography, middle row: plots of the velocity magnitude, bottom row: strain rate plots for case 4 (standard keel), case 14 (weaker margin) and case 12 (thin margin and keel), showing how the structure of the continent influences the presence of channeled flow beneath the margin, leading to a partitioning of velocities across the margin and keel and ultimately focusing of strain-rates and deformation within the continental margin.

4. Discussion

4.1. Model limitations

The presence of vertical and lateral rheological heterogeneity within the continental lithosphere clearly modulates the slab rollback behaviour, the partitioning of plate velocities across the continent, and the deformation of the overriding plate. We explored simplified models to isolate the effect of variations in the type and extent of continental heterogeneity on the deformation of the continental margin and the slab behaviour in the upper mantle. In nature, the strength of the lithosphere is expected to be controlled by a range of factors, including lithological variations, evolving grain size, and other damage memory (e.g. Hirth and Kohlstedt, 2004; Montési, 2013; Bercovici and Ricard, 2016). The implications of these contributions on effective viscosity and yield stress are only approximately represented by our relatively simple rheological setup. In particular, we do not account for a reduction in plastic yield stress with progressive deformation and thus have no true strain localisation. Were we to include localization, we would expect the difference in topography formation scenarios to be even more pronounced.

The rheology of our models is also simplified by excluding a multi-mineralic slab and mantle, and ignores the effects of phase changes. These simplifications may have important implications for the slab behaviour and slab induced viscous flow. Moreover, mantle flow in nature is, of course, 3-D and due to the restriction of our simplified models, we thus miss the toroidal flow component. The latter may play a significant role in slab rollback, upper mantle slab behaviour, and continental deformation (e.g. Stegman et al., 2006; Faccenna and Becker, 2010; Capitanio and Replumaz, 2013). While slab dynamics, including the temporal evolution of trench retreat, and the partitioning of the plate velocities may thus be affected by all of these complexities, we expect the relative effects of keels on deformation to be fairly similar.

4.2. Analogues in nature

The presence of a continental keel can delimit the extent of the back-arc deformation and constrain it to a narrow zone of subsidence and extension. When the continental keel presence is shifted towards the trench, this further spatially limits the amount of back-arc region involved in the margin deformation and subsidence. Related dynamics may explain the narrow back-arc extension observed in some subduction zones such as the Ryukyu subduction zone (e.g Faccenna et al., 2014).

We also find that a combination of weak continental margins and strong, extended keels favour wide zones of deformation and extensive subsidence. These margins also exhibit multiple basins and significant asymmetry reflecting the partitioning of the asthenospheric drag underneath the continental margin, and the splitting of the overriding plate velocity within the continental margin. Models with wide zones of back-arc deformation also record the highest amount of trench rollback. This behaviour is consistent with the highly extended, asymmetric back-arc deformation observed in the Pannonian and Aegean basins (Wortel, 2000; Faccenna et al., 2014) which also record multiple basins and considerable subsidence. This suggests that these Mediterranean back-arcs involve in combination or separately, rheologically weaker continental lithosphere and/or stronger or more extensive continental keels. Together with high convergence rates and fast slab rollback may contribute to the extensive thinning and extension of the continental margin.

The properties of the continental keel can also contribute to the uplift of the continental margin. In case 8 (Fig. 7), a denser than standard (for our models) continental keel produces a neutrally buoyant continental lithosphere and an isostatically uplifted continental margin. The overall uplift signal is recorded within a relatively narrow back-arc region similar to that of cases 4, 5, and 9 (Fig. 7). The uplifted margin in keel-case 8 also records a central, narrow and shallow basin suggesting an analogy to the Andean intermontane basins (Horton, 2005) and the late Cretaceous to early Paleogene intermontane basins of the Laramide orogeny in the Basin and Range area, and around the Colorado Plateau (Lawton, 2019).

5. Conclusions

The structure of the overriding continental plate directly influences the evolution of topography and deformation within the continental margin. Variations in keel and margin properties also modulate the slab behaviour, the amount of trench retreat, and the partitioning of the slab-induced flow across the continental margin and between the margin and the continental interior.

Wide zones of deformation and extensive subsidence form within the continental margin and back-arc regions when the continental keel is strong and extended, and the margins are weak. Thin, spatially limited keels, and strong margins produce narrow back-arc margins. In nature, back-arc extension and subsidence may thus not only reflect convergence kinematics and local structure, but may also be affected by the adjacent continental lithosphere.

Large extended back-arc regions such as the Pannonian and the Aegean back-arcs may be a result of an interplay between fast slab rollback and a weak continental margin combined with a strong and extended continental keel. Narrow margins such as the Okinawa trough in NE Japan may be indicative of a comparatively stronger continental margin and weaker and/or smaller continental keel. Continental keel properties can also influence the uplift of the deformation front and encourage the formation of intermontane basins in regions such as the Andes and within the Laramide orogeny.

Our study underscores the importance of considering heterogeneities in the continental lithosphere, such as keel and margin properties, when investigating subduction zone dynamics. Further, integrative modeling adapted to real-world subduction systems should contribute to a more comprehensive understanding of the complex interactions between oceanic plate subduction and the highly variable continental lithosphere.

Acknowledgments

TWB was partially supported by NSF EAR 1925939 and 2045292, and computations were performed on the NSF supercomputer *Frontera* at the Texas Advanced Computing Center. We thank the developers and Computational Infrastructure for Geodynamics (geodynamics.org) which is funded by the National Science Foundation under award EAR-0949446 and EAR-1550901 for supporting the development of ASPECT.

Appendix A. Appendix

Appendix A.1. The Top Boundary Condition Question - Free Slip or Free Surface?

We explore the influence of a free surface and free slip top boundary condition on the evolution of topopgraphy, continental extension, trench retreat, and slab behaviour for cases 1-4 (Table A.2). For keel-free-case 1, there is little variation between the free surface and the free slip implementations for the slab morphology both at 20 Myrs when the slab is in the upper mantle, and also at 80 Myrs when the slab has sunk into the lower mantle. Strain rates are also similar and the topography at the surface is comparable save for minor, small-scale features (Fig. A.10). For reference-keel-case 2 we maintain a similar continental lithosphere thickness but introduce a 75 km thick, higher viscosity continental keel (Table A.2) at the bottom of the continental lithosphere. We find that similar to test case 1, in test case 2 there is very little variation in the slab morphology, strain rates, or topography recorded throughout the model evolution for both the free surface and the free slip cases.

Next, in keel-free-case 3, we further explore the effects of vertical viscosity variations by introducing a viscosity reduction of an order of magnitude within the bottom 50 km of the continental lithosphere (Table A.2 and sec. 2.3). We find that for these models the nature of the top boundary condition of the model is important and can result in significant differences in strain rates and in the evolution of the continental topography for the free

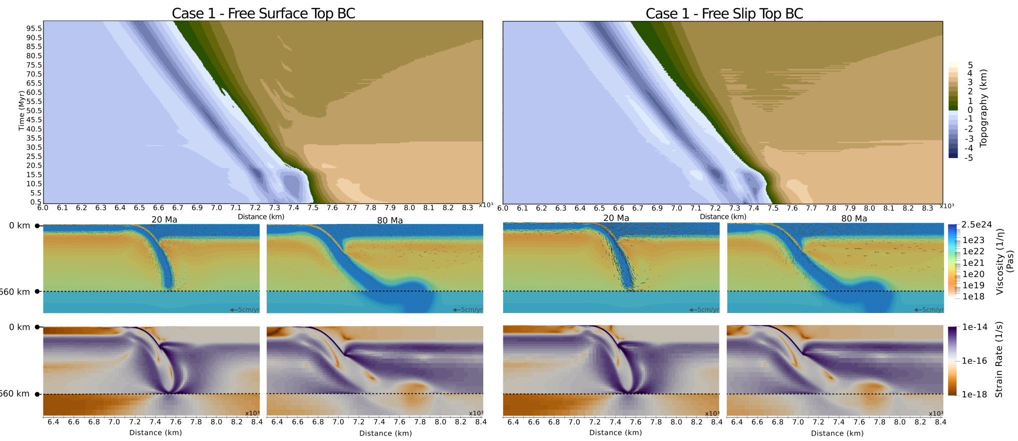

Figure A.10: Surface boundary conditions for keel-free-case 1 models with initial homogeneous continental η implementation. Left: Free surface boundary condition. Right: Free slip boundary condition. Top row: Topography; middle row: viscosity and induced viscous flow velocity; bottom row: strain rates

surface and free slip versions. Fig. A.12 clearly shows that for test case 3 the free surface implementation exhibits significant focusing of higher strain rates within the continental lithosphere for the first 30 Myrs of model evolution. This produces significant topographic contrast with multiple horst and graben-like features on the overriding plate which eventually coalesce into broader wavelength zones of higher and lower topography. These variations in topography and strain rates within the overriding plate are missing in the same model set-up with a free slip top boundary condition (Fig. A.12). However, slab behaviour across the two set-ups is similar.

In keel-case 4 we include a continental keel similar to that of case 2 and maintain a viscosity reduction similar to case 3 but limit this to the keel-free margin of the continental lithosphere (secs. A.2 and 2.3). Comparing the free

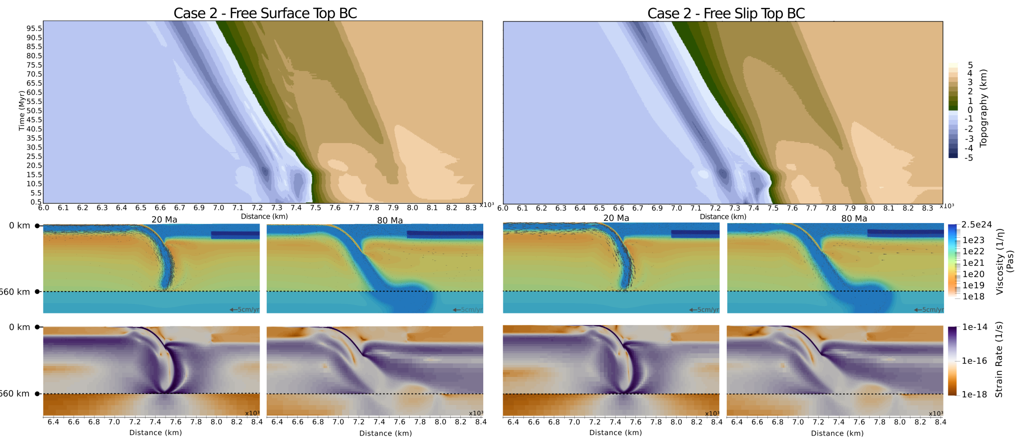

Figure A.11: Surface boundary conditions for reference-keel-case 2 models with initial homogeneous continental η and continental keel implementation. Left: Free surface boundary condition. Right: Free slip boundary condition. Top row: Topography; middle row: viscosity and induced viscous flow velocity; bottom row: strain rates

surface and free slip versions of test case 4 we find that similar to test case 3 the nature of the top boundary condition plays a significant role in both the strain rates and their focusing, as well as the evolution of topography at the surface. Here too, we observe strain rate focusing within the keel-free ~200 km continental margin, leading to the development of a well-defined central basin bounded by two areas of higher topography on either side. This topographic signal is maintained through the model evolution, even as the continental overriding plate undergoes overall subsidence. The free slip version of this set-up is missing both the focusing of the higher strain rates within the continental margin (i.e. the keel-free space between the continental edge and the keel edge) and the formation of a central basin bounded by two shoulders of higher topography (Fig. A.13). Similar to test cases 1-3, slab

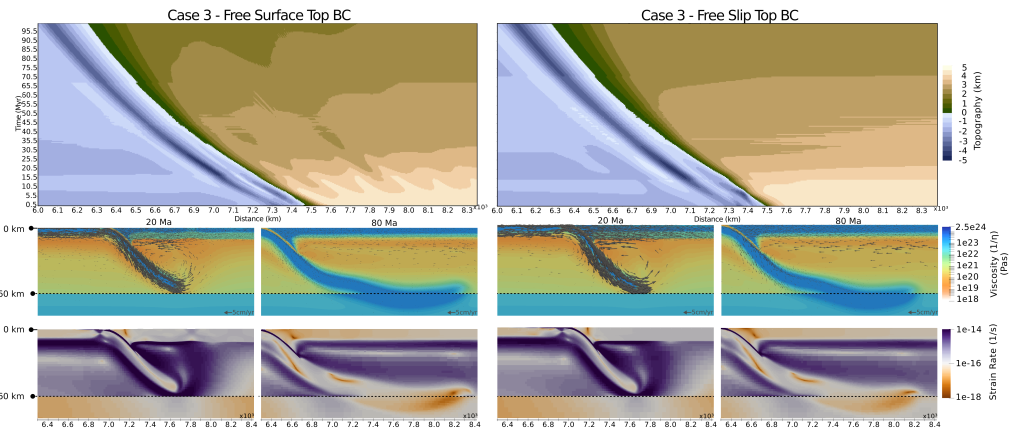

Figure A.12: Surface boundary conditions for keel-free-case 3 models with continental η variations. Left: Free surface boundary condition. Right: Free slip boundary condition. Top row: Topography; middle row: viscosity and induced viscous flow velocity; bottom row: strain rates

morphology in test case 4 does not seem to be impacted by the type of the top boundary condition implemented.

For this study we first test the impact of top boundary conditions on the evolution of topography and slab dynamics in cases 1-4. We then analyze the role of variations in continental keel properties (cases 4-10) and continental margin properties (cases 11 -14). The variations tested are detailed in Table A.2. Continental heterogeneity has a first-order impact on the margin subsidence and extent, the number of basins within the back-arc region, the elevation change within the continental interior, the trench depth, and the trench rollback described in Table A.3 for each model tested.

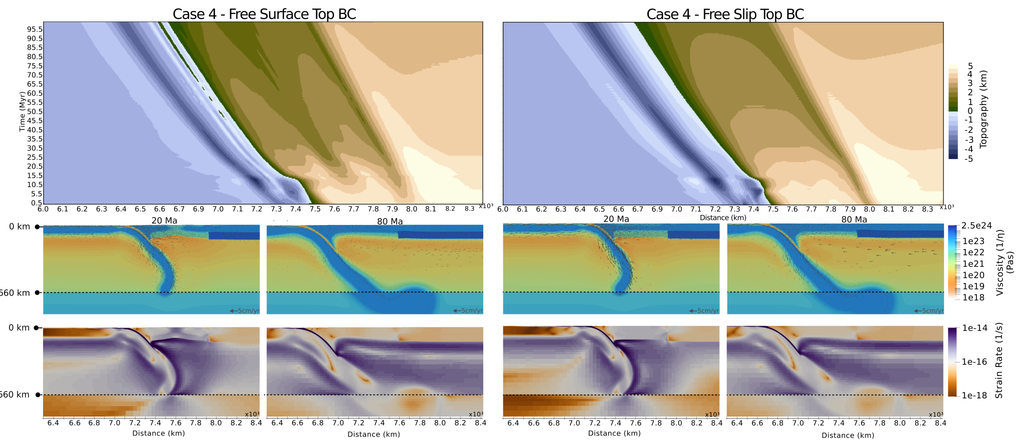

Figure A.13: Surface boundary conditions for keel-case 4 models with continental η variations and keel implementation. Left: Free surface boundary condition. Right: Free slip boundary condition. Top row: Topography; middle row: viscosity and induced viscous flow velocity; bottom row: strain rates

Model	**Lower OP η (Pa s)**	**Lower OP T (K)**	**Keel Thickness (km)**	**Keel Length (km)**	**Keel η (Pa s)**	**Keel ρ (kg m^{-3})**	**Margin Thickness (km)**	**Margin Extent (km)**	λ
Case 1	$2.5 \cdot 10^{23}$	500	N/A	N/A	N/A	N/A	N/A	N/A	N/A
Case 2	$2.5 \cdot 10^{23}$	500	75	200	$2.5 \cdot 10^{24}$	3150	150	200	0.5
Case 3	$2.5 \cdot 10^{21}$	1573	N/A	N/A	N/A	N/A	N/A	N/A	N/A
Case 4	$2.5 \cdot 10^{21}$	1573	75	200	$2.5 \cdot 10^{24}$	3150	150	200	0.5
Case 5	$2.5 \cdot 10^{21}$	1573	100	200	$2.5 \cdot 10^{24}$	3150	150	200	0.5
Case 6	$2.5 \cdot 10^{21}$	1573	50	200	$2.5 \cdot 10^{24}$	3150	150	200	0.5
Case 7	$2.5 \cdot 10^{21}$	1573	75	900	$2.5 \cdot 10^{24}$	3150	150	200	0.5
Case 8	$2.5 \cdot 10^{21}$	1573	75	200	$2.5 \cdot 10^{24}$	3330	150	200	0.5
Case 9	$2.5 \cdot 10^{21}$	1573	75	200	$2.5 \cdot 10^{26}$	3150	150	200	0.5
Case 10	$2.5 \cdot 10^{21}$	1573	75	900	$2.5 \cdot 10^{26}$	3150	150	200	0.5
Case 11	$2.5 \cdot 10^{21}$	1573	75	200	$2.5 \cdot 10^{24}$	3150	150	150	0.5
Case 12	$2.5 \cdot 10^{21}$	1573	50	200	$2.5 \cdot 10^{24}$	3150	100	200	0.5
Case 13	$2.5 \cdot 10^{21}$	1573	75	200	$2.5 \cdot 10^{24}$	3150	150	200	0.3
Case 14	$2.5 \cdot 10^{21}$	1573	75	200	$2.5 \cdot 10^{24}$	3150	150	200	0.07

Table A.2: Keel and margin variations for models with a free surface and a free slip top boundary condition, where OP is the overriding plate

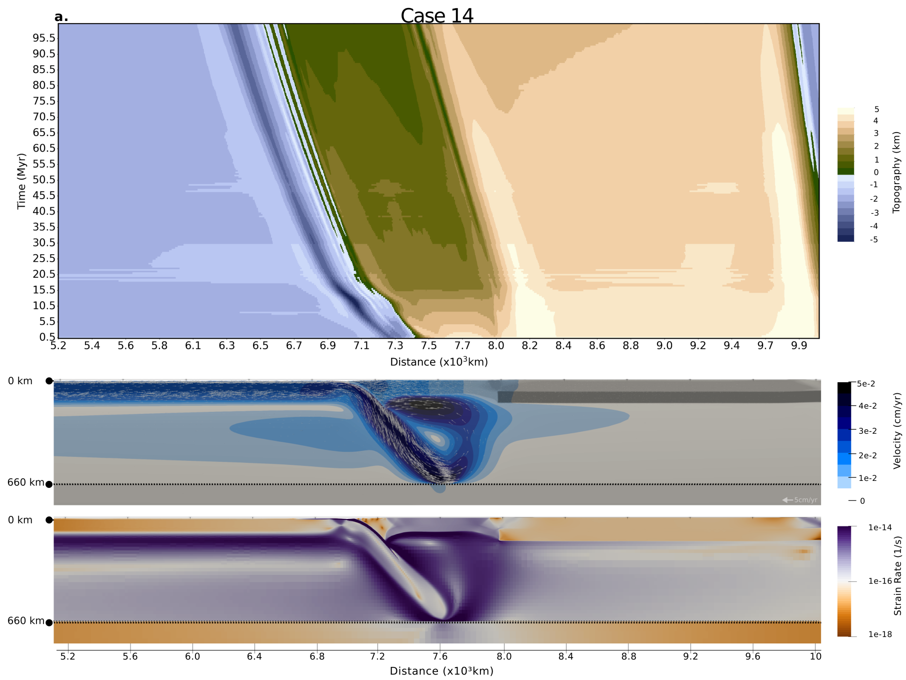

Figure A.14: Zoomed in view for Fig. 9 showing the free surface topography, the velocity magnitude and strain rate for case 14 (weaker margin). Note the strain-focusing patterns following the velocity partitioning within the continental margin and the shear bands linking the central subsidence with the margin shoulders

Model	Margin Subsidence (km)	Margin Extent (km)	Number of Margin Basins	Interior Elevation Change (km)	Trench Depth (km)	Trench rollback (km)
Case 4	3	260	1	1.5	4	860
Case 5	3.5	280	1	1	3.25	790
Case 6	1.5	75	0	1	2.5	475
Case 7	3.5	360	3	1.5	4	890
Case 8	3	310	1	1.5	3.3	760
Case 9	3.5	320	3	1	3.7	725
Case 10	4.5	440	3	1	3.15	710
Case 11	2.5	60	3	1.5	3.75	755
Case 12	1	50	0	1	3.1	580
Case 13	3	195	0	1.5	3.3	805
Case 14	3.5	430	2	1.5	3.89	990

Table A.3: Subduction parameters measured for models with keel variations (cases 4-10) and margin variations (cases 11-14)

References

Audet, P., Bürgmann, R., 2011. Dominant role of tectonic inheritance in supercontinent cycles. Nature Geosc. 4, 184–187.

Balázs, A., Burov, E., Matenco, L., Vogt, K., Francois, T., Cloetingh, S., 2017. Symmetry during the syn- and post-rift evolution of extensional back-arc basins: The role of inherited orogenic structures. Earth and Planetary Science Letters 462, 86–98. doi:10.1016/j.epsl.2017.01.015.

Bangerth, W., Dannberg, J., Fraters, M., Gassmoeller, R., Glerum, A., Heister, T., Naliboff, J., 2021. Aspect v2.3.0. URL: `https://doi.org/10.5281/zenodo.5131909`, doi:10.5281/zenodo.5131909.

Becker, T.W., 2006. On the effect of temperature and strain-rate dependent viscosity on global mantle flow, net rotation, and plate-driving forces. Geophys. J. Int. 167, 943–957. doi:10.1111/j.1365-246X.2006.03172.x.

Behr, W.M., Holt, A.F., Becker, T.W., Faccenna, C., 2022. The effects of plate interface rheology on subduction kinematics and dynamics. Geophys. J. Int. 230, 796–812. doi:10.1093/gji/ggac075.

Bercovici, D., Ricard, Y., 2016. Grain-damage hysteresis and plate tectonic states. Phys. Earth Planet. Int. 253, 31–47.

Billen, M.I., Hirth, G., 2005. Newtonian versus non-Newtonian upper mantle viscosity: Implications for subduction initiation. Geophys. Res. Lett.

32, n/a–n/a. URL: http://doi.wiley.com/10.1029/2005GL023457, doi:10.1029/2005GL023457.

Butterworth, N.P., Quevedo, L., Morra, G., Müller, R.D., 2012. Influence of overriding plate geometry and rheology on subduction. Geochemistry, Geophysics, Geosystems 13, n/a–n/a. URL: http://doi.wiley.com/10.1029/2011GC003968, doi:10.1029/2011GC003968.

Capitanio, F.A., Replumaz, A., 2013. Subduction and slab breakoff controls on Asian indentation tectonics and Himalayan western syntaxis formation. Geochem., Geophys., Geosys. 14, 3515–3531.

Capitanio, F.A., Stegman, D.R., Moresi, L., Sharples, W., 2010. Upper plate controls on deep subduction, trench migrations and deformations at convergent margins. Tectonophys. 483, 80–92.

Chase, C.G., 1978. Extension behind island arcs and motions relative to hot spots. Journal of Geophysical Research 83, 5385. doi:10.1029/jb083ib11p05385.

Conrad, C.P., Lithgow-Bertelloni, C., 2006. Influence of continental roots and asthenosphere on plate-mantle coupling. Geophysical Research Letters 33, L05312. URL: http://doi.wiley.com/10.1029/2005GL025621, doi:10.1029/2005GL025621.

Crameri, F., Lithgow-Bertelloni, C., 2018. Abrupt upper-plate tilting during slab-transition-zone collision. Tectonophysics 746, 199–211. URL: https://doi.org/10.1016/j.tecto.2017.09.013, doi:10.1016/j.tecto.2017.09.013.

Dasgupta, R., Mandal, N., Lee, C., 2021. Controls of subducting slab dip and age on the extensional versus compressional deformation in the overriding plate. Tectonophysics 801, 228716. URL: https://doi.org/10.1016/j.tecto.2020.228716, doi:10.1016/j.tecto.2020.228716.

Enns, A., Becker, T.W., Schmeling, H., 2005. The dynamics of subduction and trench migration for viscosity stratification. Geophys. J. Int. 160, 761–775.

Erdős, Z., Huismans, R.S., Faccenna, C., 2022. Wide versus narrow back-arc rifting: Control of subduction velocity and convective back-arc thinning. Tectonics 41. doi:10.1029/2021TC007086.

Faccenna, C., Becker, T.W., 2010. Shaping mobile belts by small-scale convection. Nature 465, 602–605. URL: http://dx.doi.org/10.1038/nature09064, doi:10.1038/nature09064.

Faccenna, C., Becker, T.W., Auer, L., Billi, A., Boschi, L., Brun, J.P., Capitanio, F.A., Funiciello, F., Horvàth, F., Jolivet, L., Piromallo, C., Royden, L., Rossetti, F., Serpelloni, E.,

2014. Mantle dynamics in the Mediterranean. Rev. Geophys. 52, 283–332. URL: http://doi.wiley.com/10.1002/2013RG000444, doi:10.1002/2013RG000444.

Garel, F., Goes, S., Davies, D.R., Davies, J.H., Kramer, S.C., Wilson, C.R., 2014. Interaction of subducted slabs with the mantle transition-zone: A regime diagram from 2-D thermo-mechanical models with a mobile trench and an overriding plate. Geochemistry, Geophys. Geosystems 15, 1739–1765. URL: https://onlinelibrary.wiley.com/doi/10.1002/2014GC005257, doi:10.1002/2014GC005257.

Ghosh, A., Becker, T.W., Zhong, S.J., 2010. Effects of lateral viscosity variations on the geoid. Geophysical Research Letters 37. doi:10.1029/2009GL040426.

Ghosh, A., Holt, W., Wen, L., 2013. Predicting the lithospheric stress field and plate motions by joint modeling of lithosphere and mantle dynamics. Journal of Geophysical Research: Solid Earth 118, 346–368.

Gordon, R.G., 2000. Diffuse oceanic plate boundaries: Strain rates, vertically averaged rheology, and comparisons with narrow plate boundaries and stable plate interiors, in: Richards, M.A., Gordon, R.G., van der Hilst, R.D. (Eds.), The History and Dynamics of Global Plate Motion. American Geophysical Union, Washington DC. volume 121 of *Geoophys. Mono.*, pp. 143–159.

Hager, B.H., 1984. Constraints on Mantle Rheology and Flow Residual Geoid: degree 2-10. J. Geophys. Res. 89, 6003–6015.

Heister, T., Dannberg, J., Gassmöller, R., Bangerth, W., 2017. High accuracy mantle convection simulation through modern numerical methods. II: Realistic models and problems. Geophysical Journal International 210, 833–851. URL: https://doi.org/10.1093/gji/ggx195, doi:10.1093/gji/ggx195.

Heuret, A., Funiciello, F., Faccenna, C., Lallemand, S., 2007. Plate kinematics, slab shape and back-arc stress: A comparison between laboratory models and current subduction zones. Earth Planet. Sci. Lett. 256, 473–483. doi:10.1016/j.epsl.2007.02.004.

Heuret, A., Lallemand, S., 2005. Plate motions, slab dynamics and back-arc deformation. Physics of the Earth and Planetary Interiors 149, 31–51. URL: https://linkinghub.elsevier.com/retrieve/pii/S0031920104003462, doi:10.1016/j.pepi.2004.08.022.

Hirth, G., Kohlstedt, D., 2004. Rheology of the upper mantle and the mantle wedge: A view from the experimentalists. Geophys. Monogr. Ser. 138, 83–105. doi:10.1029/138GM06.

Holt, A.F., Becker, T.W., Buffett, B.A., 2015a. Trench migration and overriding plate stress in dynamic subduction models. Geophysical Journal International 201, 172–192. doi:10.1093/gji/ggv011.

Holt, A.F., Buffett, B.A., Becker, T.W., 2015b. Overriding plate thickness control on subducting plate curvature. Geophysical Research Letters 42, 3802–3810. doi:10.1002/2015GL063834.

Holt, A.F., Condit, C.B., 2021. Slab Temperature Evolution Over the Lifetime of a Subduction Zone. Geochemistry, Geophys. Geosystems 22. doi:10.1029/2020GC009476.

Horton, B.K., 2005. Revised deformation history of the central andes: Inferences from cenozoic foredeep and intermontane basins of the eastern cordillera, bolivia. doi:10.1029/2003TC001619.

Jordan, T., 1981. Continents as a chemical boundary layer. Phil. Trans. Royal Soc. London. A 301, 359–373.

Kaus, B.J.P., Steedman, C., Becker, T.W., 2008. From passive continental margin to mountain belt: insights from analytical and numerical models and application to Taiwan. Phys. Earth Planet. Inter. 171, 235–251.

King, S.D., Masters, G., 1992. Scott D. King x and Guy Masters. Geophys. Res. Lett. 19, 1551–1554.

Kronbichler, M., Heister, T., Bangerth, W., 2012. High accuracy mantle convection simulation through modern numerical methods. Geophysical Journal International 191, 12–29.

URL: http://dx.doi.org/10.1111/j.1365-246X.2012.05609.x, doi:10.1111/j.1365-246X.2012.05609.x.

Lallemand, S., Heuret, A., 2017. Subduction zones parameters . doi:10.1016/B978-0-12-409548-9.09495-1.

Lawton, T.F., 2019. Laramide sedimentary basins and sediment-dispersal systems. doi:10.1016/B978-0-444-63895-3.00013-9.

Lee, C.T.A., Lenardic, A., Cooper, C.M., Niu, F., Levander, A., 2005. The role of chemical boundary layers in regulating the thickness of continental and oceanic thermal boundary layers. Earth Planet. Sci. Lett. 230, 379–395.

Lenardic, A., Moresi, L., Mühlhaus, H., 2000. The role of mobile belts for the longevity of deep cratonic lithosphere: The crumple zone model. Geophys. Res. Lett. 27, 1235–1238. doi:10.1029/1999GL008410.

Lenardic, A., Moresi, L.N., Mühlhaus, H., 2003. Longevity and stability of cratonic lithosphere: Insights from numerical simulations of coupled mantle convection and continental tectonics. J. Geophys. Res. Solid Earth 108, 1–15. URL: http://doi.wiley.com/10.1029/2002JB001859, doi:10.1029/2002JB001859.

Molnar, P., Atwater, T., 1978. Interarc spreading and cordilleran tectonics as alternates related to the age of subducted oceanic lithosphere. Earth and Planetary Science Letters 41, 330–340.

Montési, L.G.J., 2013. Fabric development as the key for forming ductile shear zones and enabling plate tectonics. J. Struct. Geol. 50, 254–266.

Naliboff, J.B., Conrad, C.P., Lithgow-Bertelloni, C., 2009. Modification of the lithospheric stress field by lateral variations in plate-mantle coupling. Geophysical Research Letters 36. doi:10.1029/2009GL040484.

O'Driscoll, L.J., Humphreys, E.D., Saucier, F., 2009. Subduction adjacent to deep continental roots: Enhanced negative pressure in the mantle wedge, mountain building and continental motion. Earth Planet. Sci. Lett. 280, 61–70.

Paul, J., Conrad, C.P., Becker, T.W., Ghosh, A., 2023. Convective self-compression of cratons and the stabilization of old lithosphere. Geophys. Res. Lett. 50. doi:10.1029/2022GL101842.

Pearson, D.G., Scott, J.M., Liu, J., Schaeffer, A., Wang, L.H., van Hunen, J., Szilas, K., Chacko, T., Kelemen, P.B., 2021. Deep continental roots and cratons. doi:10.1038/s41586-021-03600-5.

Rolf, T., Tackley, P.J., 2011. Focussing of stress by continents in 3D spherical mantle convection with self-consistent plate tectonics. Geophys. Res. Lett. 38. doi:10.1029/2011GL048677.

Sandiford, D., Brune, S., Glerum, A., Naliboff, J., Whittaker, J.M., 2021. Kinematics of Footwall Exhumation at Oceanic Detachment faults:

Solid-Block Rotation and Apparent Unbending. Geochemistry, Geophys. Geosystems 22, 1–12. doi:10.1029/2021GC009681.

Sdrolias, M., Müller, R.D., 2006. Controls on back-arc basin formation. Geochemistry, Geophysics, Geosystems 7. doi:10.1029/2005GC001090.

Sharples, W., Jadamec, M.A., Moresi, L.N., Capitanio, F.A., 2014. Overriding plate controls on subduction evolution. Journal of Geophysical Research: Solid Earth 119, 6684–6704. URL: https://onlinelibrary.wiley.com/doi/abs/10.1002/2014JB011163, doi:10.1002/2014JB011163.

Sleep, N., Toksöz, M.N., 1971. Evolution of marginal basins. Nature 233, 548–550.

Stegman, D.R., Freeman, J., Schellart, W.P., Moresi, L.N., May, D., 2006. Influence of trench width on subduction hinge retreat rates in 3-D models of slab rollback. Geochem., Geophys., Geosys. 7. doi:10.1029/2005GC001056.

Sternai, P., Jolivet, L., Menant, A., Gerya, T., 2014. Driving the upper plate surface deformation by slab rollback and mantle flow. Earth and Planetary Science Letters 405, 110–118. URL: http://dx.doi.org/10.1016/j.epsl.2014.08.023, doi:10.1016/j.epsl.2014.08.023.

Uyeda, S., 1982. Subduction zones: An introduction to comparative subductology. Tectonophysics 81, 133–159.

Wolf, S.G., Huismans, R.S., 2019. Mountain building or backarc extension in ocean-continent subduction systems: A function of backarc lithospheric strength and absolute plate velocities. Journal of Geophysical Research: Solid Earth 124, 7461–7482. doi:10.1029/2018JB017171.

Wortel, M.J.R., 2000. Subduction and Slab Detachment in the Mediterranean-Carpathian Region. Science (80-.). 290, 1910–1917. URL: http://www.sciencemag.org/cgi/doi/10.1126/science.290.5498.1910, doi:10.1126/science.290.5498.1910.

Yoshida, M., 2012. Dynamic role of the rheological contrast between cratonic and oceanic lithospheres in the longevity of cratonic lithosphere: A three-dimensional numerical study. Tectonophys. 532, 156–166.

Zhong, S., 2001. Role of ocean-continent contrast and continental keels on plate motion, net rotation of lithosphere, and the geoid. Journal of Geophysical Research: Solid Earth 106, 703–712. doi:10.1029/2000jb900364.